Macromolecules

pubs.acs.org/Macromolecules Article

Hierarchical Self-Assembly of ABC-Type Bottlebrush Copolymers

Qingliang Song, Qingshu Dong, Ruiqi Liang, Yazhen Xue, Mingjiang Zhong,* and Weihua Li*

Cite This: https://doi.org/10.1021/acs.macromol.3c00440 Read Online

ACCESS | Metrics & More | Article Recommendations | Supporting Information

ABSTRACT: We have performed dissipative particle dynamics simulations to study the self-assembly of ABC-type bottlebrush copolymers (BBCPs), one portion of whose backbone is grafted by pairs of A-blocks and the other portion is grafted by B/C-blocks in pairs, focusing on the effects of the number of A side chains, the length of B side chains relative to that of C side chains, and the rigidity of the backbone on the formation of hierarchical structures. A number of hierarchical structures with the superstructures formed by the phase separation between A and B/C-blocks and the substructures formed by the phase separation between B and C-blocks are observed. Some hierarchical structures are similar to those self-assembled by ABC star copolymers, whereas their stable parameter regions of ABC-type BBCPs are much larger. On the other hand, the ABC-type BBCPs can also form some novel hierarchical structures that are hard to form in ABC star copolymers. Though the formation of the A-superstructure and the B-substructure in many hierarchical structures can be independently controlled, there are also some hierarchical structures in which the transitions of the superstructure and substructures are coupled. In other words, the A-superstructure changes along with the transformation of the B-substructure for fixed f_A. In addition, our results demonstrate that the rigidity of the backbone has a significant effect on the formation of the hierarchical structure in ABC-type BBCPs, i.e., a rigid backbone favors the normal arrangement of B-substructures to A-superstructures. Our work not only deepens the understanding of the self-assembly mechanism of ABC-type BBCPs but also provides helpful guidance for experiments to fabricate interesting hierarchical structures.

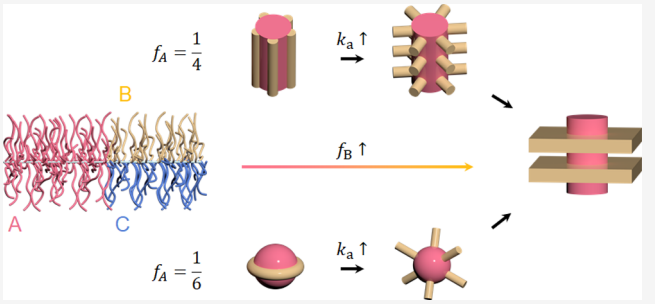

INTRODUCTION

The self-assembly of block copolymers has been attracting intensive interest as it can form a variety of ordered nanostructures with length scales typically in the range of 10−100 nm.[1−4] The self-assembly behavior of the AB diblock copolymer, which is the simplest block copolymer, is mainly controlled by two parameters, i.e., the volume fraction of A-block (f) and the product χN, where N is the number of monomers and χ is the Flory−Huggins parameter quantifying the immiscibility between A and B-blocks. The formation of the equilibrium structure is dictated by the delicate balance between the two tendencies of minimizing the interaction energy and maximizing the chain configurational entropy. As f decreases from 0.5 to 0, the AB diblock copolymer self-assembles into a few ordered phases in sequence, mainly including lamellae, bicontinuous double-gyroid network, a hexagonal array of cylinders, and a body-centered-cubic lattice of spheres.[5,6]

For polymers, one important variable is their controllable architecture. In particular, as modern synthesis techniques advance, a large multitude of chain architectures can be accessed.[7−11] Chain architectures have been made full use of to modulate the properties of polymeric materials. Indeed, the chain architecture plays an irreplaceable role in controlling the self-assembly behavior of block copolymers.[4,12−14] In the past few decades, block copolymers with different architectures have been extensively studied by experiment and theory. Novel structures were experimentally obtained from the self-assembly of architecture-engineered block copolymers.[15−23] Accordingly, these experimental results promoted theoretical studies to explore the self-assembly mechanism of these new block copolymers.[24−33] In particular, recent theoretical works have been devoted to achieving nonclassical ordered structures by purposely designing the architectures of block copolymers,[27,33−39] and great progress has been made. For example, the spherical phase region has been largely expanded by tailoring the asymmetric architectures of AB-type block copolymers, stabilizing complex Frank−Kasper spherical phases.[27,36−38] The synergistic effect of the released packing frustration and stretched bridging block has been applied to stabilize many nonclassical low-coordinated phases, such as simple cubic spheres and square cylinders.[40] Encouragingly, some theoretical predictions have been confirmed. Ahn et al.

Received: March 8, 2023
Revised: June 17, 2023

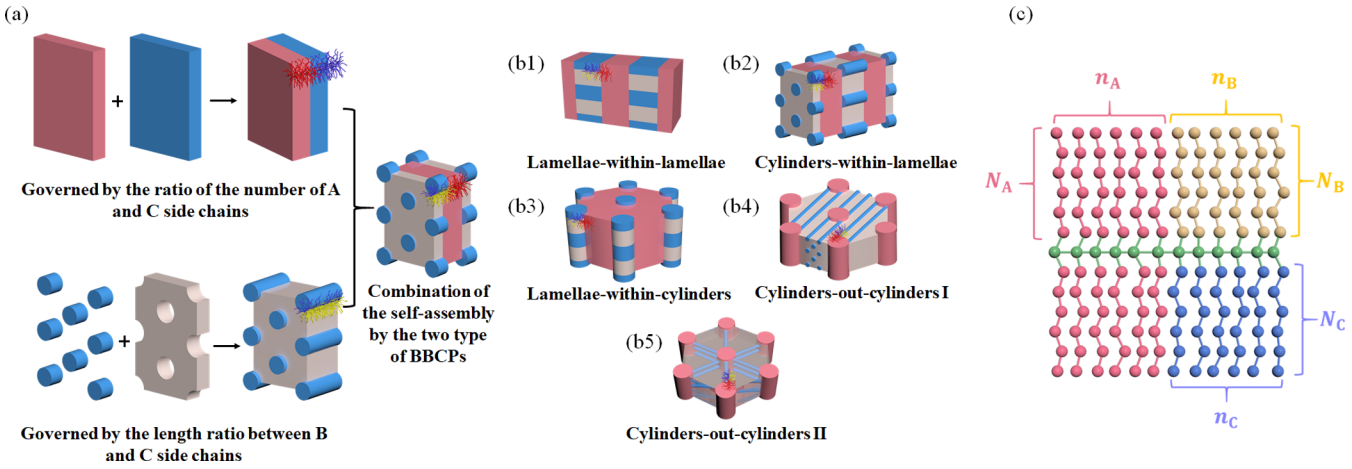

Figure 1. (a) Schematics illustrating the self-assembly of ABC-type bottlebrush copolymers into cylinders-within-lamellae hierarchical structures. Since the ABC-type bottlebrush architecture can be seen as the combination of the Janus-type and diblock-type architectures, its self-assembled structure may be deduced from the self-assembled structures of the two constituent bicomponent bottlebrush copolymers. Red, yellow, and blue represent A, B, and C components, respectively. (b) Schematics illustrating the possible morphologies of self-assembled ABC-type bottlebrush copolymers. (c) DPD model of the considered ABC-type bottlebrush copolymer, where red, yellow, blue, and green beads represent A, B, C, and D (backbone) monomers, respectively. Each D-bead is tethered by a pair of A side chains or by a pair of B and C side chains.

synthesized the ABAB tetrablock copolymer of symmetric volume fractions and observed a transition sequence from lamella to cylinder to gyroid and back to lamella along lengthening the middle B-block, which was predicted by the self-consistent field theory (SCFT).[41] Seo et al. experimentally confirmed that the phase boundaries of the $A(AB)_3$ copolymer can be largely tuned by changing the length ratio of the two different A-blocks.[20] The concerted interplay between experimental and theoretical studies has accelerated the study on the self-assembly of block copolymers, thereby deepening the understanding of the self-assembly mechanisms.

One class of chain architectures that has recently emerged and attracted special research interest in experiments is the bottlebrush-like polymer.[7,8,11,14,29,42−51] The bottlebrush copolymer (BBCP) is composed of two or more types of chemically distinct blocks that are grafted to a backbone.[52−54] The conformations of the backbone can be influenced by the solvent quality[55−57] as well as grafting density.[58] Usually, the backbone is densely grafted by side chains and tends to adopt extended conformations as a result of the strong excluded-volume effect between side chains, that is, effectively exhibiting a certain degree of rigidity. The rigidity of the backbone has been evidenced by the scaling relationship between the lamellar period D and the contour length L of the backbone of diblock-type BBCPs, $D \propto L^{0.9}$.[58,59] The backbone of an AB diblock-type BBCP is divided into two parts that are grafted by A and B side chains, respectively. Though some AB diblock-type BBCPs have been observed to exhibit similar self-assembly behaviors to conventional AB diblock copolymers, there is apparently another nontrivial parameter in addition to f and χN that impacts its self-assembly, i.e., the length ratio of single A and B side chains.[29,60,61] Specifically, the length asymmetry between single A and B side chains should cause some additional effect on the spontaneous curvature. It is worth mentioning that the molecular weight of AB diblock-type BBCPs can be readily increased by adding side chains without causing significant entanglement effects. Accordingly, ordered structures of large domain periods can be self-assembled by high-molecular-weight BBCPs, which can be used as photonic crystals[8,62−66] or templates of photonic crystals.[67,68] In addition to diblock-type BBCPs, there is another AB-type BBCP, where A and B side chains are tethered to the backbone in a Janus-type architecture.[11,69−71] Since A and B side chains tend to phase-separate with the backbone residing at the A/B interface, this new type of BBCP is referred to as the Janus type. As long as the Janus-type BBCP contains enough side chains, it can phase-separate into ordered structures even for very short side chains. Contrary to diblock-type BBCPs, the Janus-type BBCPs can be used to generate ordered structures with a very small domain spacing.[11,69]

Inspired by these unique features of BBCPs, BBCPs with higher-order structure complexity have been designed and synthesized. Very recently, Liang et al. developed a multicomponent BBCP containing chemically distinct blocks (A, B, and C). The A side chains are grafted to one portion of the backbone, while the B and C side chains are tethered to the other portion in a Janus-type architecture. The basic design idea adopted by them is that the self-assembly of the multicomponent BBCPs can be regarded as the combination of assemblies by diblock-type BBCP and Janus-type BBCP (Figure 1a). In other words, the combined architecture of BBCPs can form a hierarchical structure, whose superstructure is formed by the phase separation between A-blocks and B/C-blocks, while the substructure is generated from the phase separation between B and C-blocks. By changing the ratio of the number of A side chains to that of B/C side chains as well as the length ratio of B and C side chains, they experimentally obtained some intriguing hierarchical structures, including lamellae-within-lamellae, cylinders-within-lamellae, lamellae-within-cylinders, and cylinders-out-cylinders[47] (Figure 1b1−b4). The arrangement of the subdomains within the superstructure for the first three hierarchical structures (Figure 1b1−b3) is relatively straightforward, while that in the last one (Figure 1b4) is more complicated. Intuitively, the cylinders-out-cylinders structure should be composed of a hexagonal array of A-cylinders, in the matrix of which the B-blocks further aggregate into B-cylinders. Due to the special architecture of ABC-type BBCPs, the B-cylinders prefer being perpendicular to the surface of A-cylinders. On the other hand, the B-cylinders tend to be packed into a hexagonal array to minimize

https://doi.org/10.1021/acs.macromol.3c00440
Macromolecules XXXX, XXX, XXX−XXX

the packing frustration of C-blocks. The two tendencies make the arrangement of B-cylinders within the periodic interstitial space between these hexagonally arranged A-cylinders very complicated. In experiments, it is also very difficult to clearly characterize such complex hierarchical structures due to the small feature size of the substructures. Liang et al. speculated that the B-cylinders are parallelly oriented and perpendicular to the surface of A-cylinders (Figure 1b4). Then, they attempted to use computer simulations to clarify the cylinders-out-cylinders structure.[47] However, their simulations did not display the parallelly oriented arrangement of B-cylinders in the cylinders-out-cylinders structure (Figure 1b4); instead, there was another arrangement of B-cylinders radiating outward from each A-cylinder (Figure 1b5). In fact, the ABC-type BBCPs can form a number of complex hierarchical structures, where the arrangement of their substructures is hard to infer. In order to explore more complex hierarchical structures and to fully understand the self-assembly mechanism of the ABC-type BBCPs, systematic simulation studies are needed.

The above simple scenario of rationalizing the formation of the hierarchical structures in the ABC-type BBCPs is based on the assumption that the backbone is completely rigid. The rigid backbone has a strong constraint on the packing of the side chains and thus on the formation of substructures. Reasonably, if the backbone cannot bend, the B/C interface can only be oriented perpendicular to the surface of the A-superdomain, preventing some hierarchical structures (e.g., spheres-within-lamellae structure) from being formed. However, the backbone of many BBCPs with the contour length larger than the persistence length should not be ideally rigid, but semiflexible. The semiflexibility of the backbone must have a significant role in the self-assembly behaviors of BBCPs. Therefore, in this work, we systematically investigate the self-assembly of the ABC-type BBCPs using dissipative particle dynamics (DPD) simulations, focusing on the effect of three important factors: the semiflexibility of the backbone, the number of A side chains while fixing the total number of side chains, and the length ratio of B and C side chains.

MODEL AND METHOD

We consider a melt composed of n chains of ABC-type BBCPs, each of which is grafted by $2n_A$ A side chains, n_B B side chains, and n_C C side chains.

A Janus fashion between B and C beads is modeled in the same way as the model used by Salinas-Soto and Liu et al.[57,71] To avoid the difference of grafting density, the grafting density of the backbone that consists of N_D D beads is set equal for the part of the A side chains and that of B/C side chains. That is to say, each D-bead is tethered with each pair of A side chains or each pair of B and C side chains. Each A, B, and C side chain contains N_A A beads, N_B B beads, and N_C C beads, respectively (Figure 1c). Given the dense grafting of the side chains, the interactions experienced by the backbone should remain relatively constant,[59] which allows us to ignore the interactions involving the backbones. Therefore, the backbone beads do not contribute to the calculation of the volume fractions.[47,51] Accordingly, the volume fraction of i-beads (i = A, B and C) is approximately defined as $f_i = \lambda n_i \times N_i/(2n_A \times N_A + n_B \times N_B + n_C \times N_C)$, where $\lambda = 2$ for A side chains, while $\lambda = 1$ for B and C side chains.

DPD simulations are performed in the canonical ensemble. The time evolution of DPD beads with unit mass is governed by Newton's equations of motion[72−74]

$$\frac{d\mathbf{r}_i}{dt} = \mathbf{v}_i, \frac{d\mathbf{v}_i}{dt} = \mathbf{f}_i \tag{1}$$

where

$$\mathbf{f}_i = \sum_{j\neq i} (\mathbf{F}_{ij}^{C} + \mathbf{F}_{ij}^{D} + \mathbf{F}_{ij}^{R}) \tag{2}$$

The force acting on each bead contains three parts: conservative $\mathbf{F}_{ij}^{C}$, dissipative $\mathbf{F}_{ij}^{D}$, and random $\mathbf{F}_{ij}^{R}$ force. Each part is pairwise-additive, repulsive, and short-range with a cutoff at $r = 1.0$.

The conservative force $\mathbf{F}_{ij}^{C}$ is a soft-repulsive interaction acting along the line connecting the centers of two beads

$$\mathbf{F}_{ij}^{C} = \begin{cases} a_{ij}(1 - r_{ij})\hat{\mathbf{r}}_{ij} & (r_{ij} < 1) \\ 0 & (r_{ij} \geqslant 1) \end{cases} \tag{3}$$

where $\mathbf{r}_{ij} = \mathbf{r}_i - \mathbf{r}_j$ is the vector pointing from beads j to i, $r_{ij} = |\mathbf{r}_{ij}|$ denotes the distance between beads i and j, and $\hat{\mathbf{r}}_{ij} = \mathbf{r}_{ij}/|\mathbf{r}_{ij}|$ represents the unit vector pointing from beads j to i.

The repulsive interaction between beads i and j is specified as a_{ij} (i, j = A, B, C, and D). To qualitatively mimic the immiscibility between different types of monomers in the current system, the repulsive interaction parameters chosen are shown by a symmetric matrix,[47]

$$a_{ij} = \begin{pmatrix} & A & B & C & D \\ A & 25 & 50 & 50 & 0 \\ B & 50 & 25 & 150 & 0 \\ C & 50 & 150 & 25 & 0 \\ D & 0 & 0 & 0 & 25 \end{pmatrix}$$

The number density of the beads is fixed as $\rho = 3$ so that a_{ij} is related to the Flory−Huggins parameter χ by the expression $a_{ij} = 25 + 3.27\chi_{ij}$.[74]

The dissipative force $\mathbf{F}_{ij}^{D}$ is proportional to the relative velocity and takes the form

$$\mathbf{F}_{ij}^{D} = -\gamma w^{D}(r_{ij})(\hat{\mathbf{r}}_{ij}\cdot\mathbf{v}_{ij})\hat{\mathbf{r}}_{ij} \tag{4}$$

where $\mathbf{v}_{ij} = \mathbf{v}_i - \mathbf{v}_j$ is the relative velocity and γ is the friction coefficient. The random force $\mathbf{F}_{ij}^{R}$ acts as a heat source to equilibrate the thermal motion of unresolved scales and takes the form

$$\mathbf{F}_{ij}^{R} = \sigma w^{R}(r_{ij})\theta_{ij}\hat{\mathbf{r}}_{ij} \tag{5}$$

where σ is the noise level controlling the intensity of the random force and is set to be 3.[74] $\theta_{ij}(t)$ is a randomly fluctuating variable with zero mean and unit variance, satisfying Gaussian statistics

$$\langle\theta_{ij}(t)\rangle = 0 \tag{6}$$

$$\langle\theta_{ij}(t)\theta_{kl}(t')\rangle = (\delta_{ik}\delta_{jl} + \delta_{il}\delta_{jk})\delta(t - t') \tag{7}$$

The random force is related to the dissipative force so that they satisfy the fluctuation−dissipation relation[73]

$$\sigma^2 = 2\gamma k_B T \tag{8}$$

https://doi.org/10.1021/acs.macromol.3c00440
Macromolecules XXXX, XXX, XXX−XXX

The weight functions w^D and w^R provide the range of interactions for DPD particles with a common choice

$$w^D(r) = [w^R(r)]^2 = \begin{cases} (1-r)^2, & (r<1) \\ 0, & (r\geqslant 1) \end{cases} \quad (9)$$

Both dissipative force and random force act along the line of centers so that the linear and angular momenta are conservative; the combined effect of these two forces is that of a thermostat, ensuring that the simulation is performed in a canonical ensemble.

Each pair of beads on the polymeric chain is connected by a harmonic spring potential as

$$V_{bond}(r) = \frac{1}{2}k_b(r - r_b)^2 \quad (10)$$

where r_b is the reference length, r is the distance between the beads, and k_b is the spring constant. The two constants are set as $r_b = 0$ and $k_b = 4$ for the conventional blocks.[75] It should be noted that the calculation of the nonbonded conservative forces is also applied to the bonded beads.

Park et al.[58] used molecular dynamics (MD) to investigate the effect of grafting density on the domain spacing of BBCPs and their self-assembly; the approach used by them can induce backbone stiffness naturally. Due to the use of "soft potential" in the DPD model, which allows overlap between the coarse-grained beads, the evolution toward the thermodynamic equilibrium states is faster than "hard potential" model. However, the excluded-volume effect of the side chains cannot be captured by such a "soft potential" model of DPD. The steric hindrance-induced stiffness of the backbone can be incorporated by modeling it as a wormlike chain.[59,76] The fixed contour length allows the wormlike chain to handle highly extended conformations;[59] thus, the semiflexibility of the backbone is introduced by imposing a harmonic angle potential between the adjacent bonds

$$V_{angle}(\theta) = \frac{1}{2}k_a(\theta - \theta_0)^2 \quad (11)$$

where θ_0 is the equilibrium angle and is set as π. The potential strength k_a dictates the rigidity of the backbone, and $k_a = 0$, 2, and 10 are considered in this work.

The reduced unit of dimensionless time of the system is $\tau = R_c\sqrt{m/k_BT}$. The velocity–Verlet integration scheme is applied to integrate the equations of motion. The time step is set to be 0.01τ to achieve a balance between simulation stability and performance.

All of the simulated BBCP molecules are randomly positioned in the simulation box and are simulated $2 \times 10^4\tau$ to generate a disordered state. The disordered state is generated by setting a quite low value of the nonbonded interactions in the early stage of the simulation. To facilitate the formation of equilibrium hierarchical structures with multidimensional periodicity, the annealing is performed in a stepwise manner similar to the method by Horsch et al.,[77] which used the "hard potential". We found that the annealing in the "soft potential" system can reduce defects and avoid kinetic trapping efficiently in a relatively rigid system that contains cubic cage-like "monomers",[39] but the efficiency of the annealing may depend on the simulated system.

Each simulation of at least $5.4 \times 10^5\tau$ is performed to anneal each sample toward the equilibrium morphology. In addition, for a given set of parameters, we run the DPD simulations with different cubic box sizes between 20 and 40 as well as different initial conditions. The equilibrium morphology is determined when different initial conditions lead to the same morphology. Feng et al. recently developed a method to search for the bulk periodicity of hexagonal cylinders and lamellae.[78,79] However, the method may not be applicable to the current three-component system, which has multidimensional periodicity. Our simulations are performed with the GALAMOST (version 4.0.1) simulation package, which was developed and maintained by Zhu.[80]

Since the hierarchical structures are hard to be clearly identified from instantaneous configurations due to thermal fluctuations, we calculate the local concentration by performing time average on the instantaneous configurations of bead positions within one period where the morphology does not change notably. Specifically, the box is divided into $64 \times 64 \times 64$ lattices. First, we count the number of monomers α on lattice $\boldsymbol{r}$, $m_\alpha = \sum_{n=1}^{M_\alpha} H(\boldsymbol{r} - \boldsymbol{r}_i)$, where M_α is the total number of monomers α contained in the whole simulation box. $H(\boldsymbol{r} - \boldsymbol{r}_i)$ is a step function, defined as $H(\boldsymbol{r} - \boldsymbol{r}_i) = 1$ if $|\boldsymbol{r} - \boldsymbol{r}_i| \leq r_{cut}$ and $H(\boldsymbol{r} - \boldsymbol{r}_i) = 0$ otherwise. Then, the local concentration of component α on lattice $\boldsymbol{r}$ is computed by $\phi(\boldsymbol{r}) = T_\alpha(\boldsymbol{r})/[T_A(\boldsymbol{r}) + T_B(\boldsymbol{r}) + T_C(\boldsymbol{r})]$.

RESULTS AND DISCUSSION

For the ABC-type BBCPs, there are too many parameters to explore. To give prominence to some important factors, including the rigidity parameter k_a of the backbone, the numbers of various side chains, and the length ratio between B and C side chains, we purposely fix some parameters. In our DPD model, we fix the length of the backbone, i.e., the number of D beads, as 12. In other words, the total number of side chains is 24. The number of A-beads on each A side chain and the total number of beads on each pair of B and C side chains are fixed as 6 and 12, respectively. Accordingly, the self-assembly of the ABC-type BBCPs is controlled by n_A ($n_A + n_B = 12$), the length N_B of the B side chain ($N_B + N_C = 12$), and the backbone rigidity k_a.

In order to elucidate how the rigidity of the backbone is controlled by k_a, we calculate the effective Kuhn length b_K of the backbone of the ABC-type BBCPs for different values of k_a and architectural parameters in the disordered state with $a_{AB} = a_{AC} = a_{BC} = 25$ (Figure S1), using the method proposed by Liang et al.[81] For $k_a = 0$, 2, and 10, $b_K \approx 1.9$, 3.7, and 19.2. According to the ratio of the contour length to b_K, $k_a = 0$, 2, and 10 qualitatively correspond to nearly flexible, semiflexible, and rigid, respectively, which are evidenced by the snapshots of the typical conformations (Figure S1).

We first investigate the self-assembly of the ABC-type BBCPs at $k_a = 2$ and $n_A = 6$ ($n_B = n_C = 6$) by changing the length ratio of B and C side chains, $\tau = N_B/(N_B + N_C) = N_B/12$. Note that τ is also equal to the ratio of the volume fractions between B and C-blocks, i.e., $\tau = f_B/(f_B + f_C)$. Reasonably, the interface between the A-domain and the B/C-domains should be flat due to the symmetric volume fraction of $f_A = 1/2$. As expected, the lamellae-within-lamellae hierarchical structure is observed with $\tau = 1/2$ (i.e., $N_B = 6$) (upper right of Figure 2), which is denoted as $L_L^\perp$, where the "L" in the normal font size and the "L" in the subscript indicate the lamellar superstructure and substructure, respectively, while the superscript "$\perp$" represents that the substructure is perpendicular to the superstructure. When τ is reduced to 1/3 ($N_B = 4$), the

https://doi.org/10.1021/acs.macromol.3c00440
Macromolecules XXXX, XXX, XXX−XXX

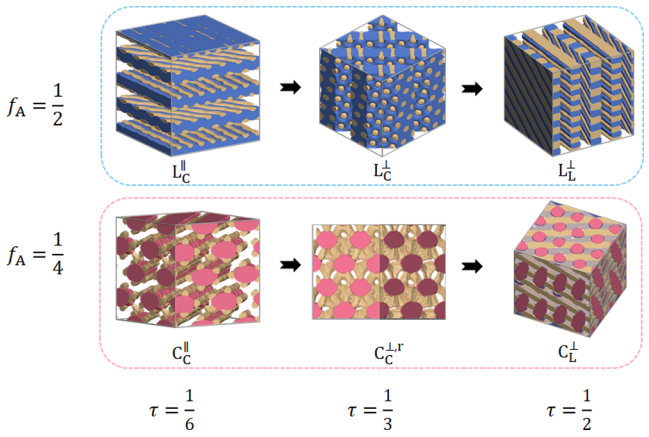

Figure 2. Hierarchical structures formed by ABC-type BBCPs at f_A = 1/2, 1/4 for τ = 1/6, 1/3, 1/2. Red, yellow, and blue represent A, B, and C components, respectively. C and L denote cylinders and lamellae, respectively.

substructure transforms from lamellae to cylinders while maintaining the lamellar superstructure (upper middle of Figure 2). The transition from lamellae-within-lamellae to cylinders-within-lamellae (denoted as $L_C^{\perp}$) is consistent with the experimental results,[47] and it is easy to understand.

As τ is reduced to 1/6 (N_B = 2), surprisingly another cylinders-within-lamellae structure ($L_C^{\parallel}$) is observed (upper left of Figure 2), where the B-cylinders are aligned parallel to the A/C interface rather than normal to the A-lamellae like those in the usual $L_C^{\perp}$ structure. In order to make B-cylinders locate on the A/C interface, the backbone has to be significantly bent, which is evidenced by the snapshot of a typical chain conformation in Figure 3a and the bending angle of the backbone in Figure 4a as well as the increased bending energy of the backbone in Figure S2. As we will see later, when the rigidity of the backbone increases, the range of τ for the formation of $L_C^{\parallel}$ will narrow and even vanish. Compared with $L_C^{\perp}$, the portion of the backbone of B/C side chains is more coiled in the $L_C^{\parallel}$ morphology (Figure 3a), giving rise to more relaxed conformations of C side chains. In other words, the formation of $L_C^{\parallel}$ gains the conformational entropy of C side chains at the expense of the bending energy of the backbone. As τ decreases or C side chains are lengthened, the conformational entropy of C side chains becomes more dominant, inducing the transition from $L_C^{\perp}$ to $L_C^{\parallel}$.

For the lamellar superstructure, the arrangement of B-domains normal to or within the surface of the A-domain is rather simple, while it becomes obviously more complicated when the A-domain becomes nonlamellar, such as cylinders. To explore the complex arrangement of B-domains within nonlamellar superstructures, we decrease f_A to 1/4 (n_A = 3) to simulate the self-assembly of the ABC-type BBCPs. At f_A = 1/4, A-blocks aggregate into hexagonally arranged cylinders (lower part in Figure 2), and the B-domain changes from a lamella to a cylinder as τ = 1/2 decreases to 1/3. Accordingly, the hierarchical structure transforms from lamellae-out-cylinders ($C_L^{\perp}$) (lower right in Figure 2) to cylinders-out-cylinders ($C_C^{\perp,r}$) (lower middle in Figure 2). In the $C_C^{\perp,r}$ structure, each piece of B-cylinder is located in the interstitial space between each pair of neighboring A-cylinders, and its orientation prefers being perpendicular to the surface of the A-cylinders at both ends as possible. As a result, a group of B-cylinders radiates outward from each A-cylinder. The superscript "r" of $C_C^{\perp,r}$ denotes the radiation distribution of B-cylinders that differs from the parallel arrangement of B-cylinders with the axial direction normal to the axial direction of A-cylinders in the cylinders-out-cylinders structure ($C_C^{\perp,\parallel}$) speculated in the previous work (Figure 1b4).[47] In the $C_C^{\perp,r}$ morphology, each B-cylinder is nearly perpendicular to the surface of the A-cylinder, allowing the bottlebrush to adopt the comfortable conformation normal to the surface of the A-cylinder. While in the $C_C^{\perp,\parallel}$ morphology, all B-cylinders are oriented along one direction perpendicular to A-cylinders, it is impossible to make these unidirectional B-cylinders be perfectly perpendicular to the circular surface of A-cylinders. This may be the reason why $C_C^{\perp,r}$ is more stable than $C_C^{\perp,\parallel}$. Similar to the transition from $L_C^{\perp}$ to $L_C^{\parallel}$, the $C_C^{\perp,r}$ structure transfers to the parallel cylinders-on-cylinders structure ($C_C^{\parallel}$) (lower left in Figure 2) as τ decreases from 1/3 to 1/6. The transition mechanism is evidenced by Figures 3b and4b as well as the increased bending energy of the backbone in Figure S2.

To gain a more complete understanding of the effect of the two control parameters (i.e., n_A and N_B) on the formation of the hierarchical structures in the ABC-type BBCPs, we construct the "phase diagram" with respect to n_A and N_B (Figure 5). The observed structures in our simulations are presented in Figure 6. Besides the two transition sequences at n_A = 6 and n_A = 3 discussed above, the phase diagram consists of more interesting phase transitions as well as some new hierarchical structures. One category of unusual transitions is the superstructural transition induced by the substructural

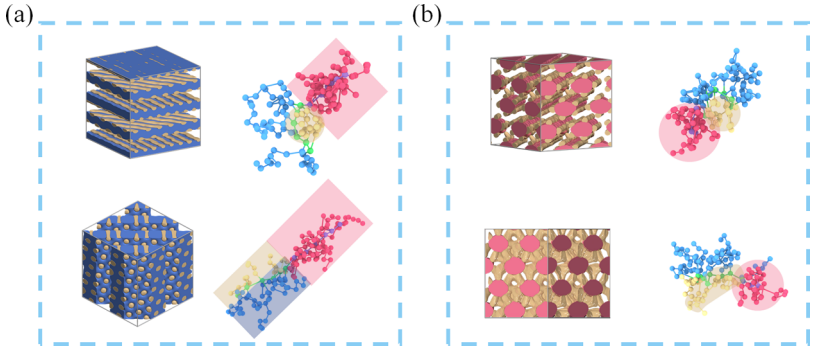

Figure 3. Hierarchical structures as well as their corresponding typical chain conformations of $L_C^{\parallel}$ (n_A = 6, N_B = 2) and $L_C^{\perp}$ (n_A = 6, N_B = 4) (a), and $C_C^{\parallel}$ (n_A = 3, N_B = 2) and $C_C^{\perp,r}$ (n_A = 3, N_B = 4) (b). Red, yellow, and blue represent A, B, and C components, respectively. For reasons of clarity, the backbone beads are divided into (blue) and (green) beads, which are grafted by A beads (red) and B(yellow)/C(blue) beads, respectively.

https://doi.org/10.1021/acs.macromol.3c00440
Macromolecules XXXX, XXX, XXX−XXX

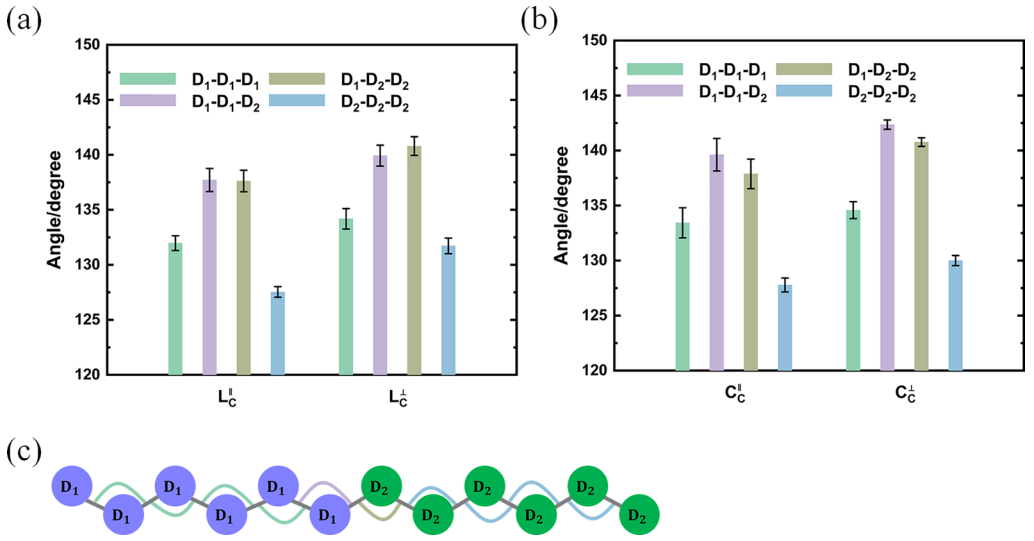

Figure 4. Comparison of the bending angle of the backbone in a pair of hierarchical structures composed of a similar superstructure and substructure but a different orientation of the substructure: $L_C^{\parallel}$ and $L_C^{\perp}$ (a) and $C_C^{\parallel}$ and $C_C^{\perp}$ (b). For reasons of clarity, the backbone beads are divided into D_1 (blue) and D_2 (green) beads, which are grafted by A beads (red) and B(yellow)/C(blue) beads, respectively (c).

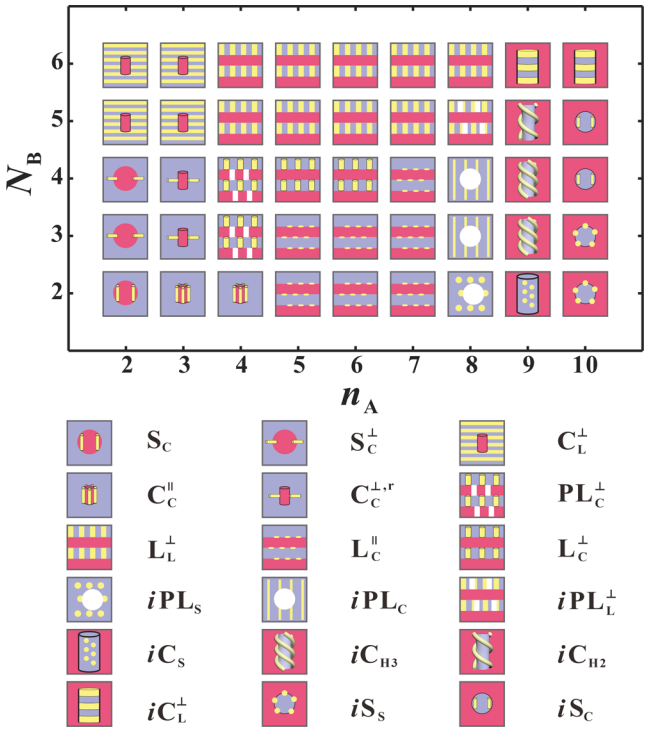

Figure 5. Phase diagram of ABC-type BBCPs with $k_a = 2$.

transition along increasing N_B for fixed n_A. For instance, at n_A = 2, the cylinders-on-spheres structure (S_C) at N_B = 2 transfers to cylinders-out-spheres ($S_C^{\perp}$) at N_B = 3 and 4 and to lamellae-out-cylinders ($C_L^{\perp}$) at N_B = 5 and 6. Along the transition from $S_C^{\perp}$ at N_B = 4 to $C_L^{\perp}$ at N_B = 5, the A-superstructure changes from a sphere to a cylinder as the B-substructure transforms from a cylinder to a lamella. The synchronous change of the superstructure is mainly to generate a translation-invariant regular space for facilitating symmetric B/C side chains to pack into the lamellar substructure. Obviously, symmetric B/C side chains can form lamellae stacked along the axial direction of aligned cylinders, but their packing becomes frustrated within the three-dimensional periodic interstitial space outside A-spheres (Figure 7a–c). A similar transition also appears at n_A = 10, i.e., the transition from cylinders-on-spheres (iS_C, where "i" indicates the inverse spherical superstructure) to lamellae-within-cylinders ($iC_L^{\perp}$) (Figure 7d–f).

Similarly, the superstructural transition accompanied by the substructural transition occurs at n_A = 4, where the parallel cylinders-out-cylinders structure ($C_C^{\parallel}$) at N_B = 2 transfers to the perpendicular cylinders-out-perforated lamellae structure ($PL_C^{\perp}$) at N_B = 3. In the $PL_C^{\perp}$ structure, the B-blocks form hexagonal cylinders within the C-matrix, and the excess C-blocks fill the holes in the A-perforated lamellae (A-PL). Indeed, the A-PL superstructure is formed under the constraint of the layering arrangement of the B/C-bottlebrush due to the rigidity of the backbone, which is similar to the formation of the PL structure in thin films.[82] Other types of perforated-lamellar superstructures are observed at n_A = 8; the spheres-within-inverse perforated lamellae (iPL_S) at N_B = 2 transfer to cylinders-within-inverse perforated lamellae (iPL_C) at N_B = 3 and 4 and to perpendicular lamellae-within-inverse perforated lamellae ($iPL_L^{\perp}$) at N_B = 5.

Another kind of interesting hierarchical structure observed is the helices-on-cylinders structure at $3 \le N_B \le 5$ and n_A = 9. The helical substructure transforms from triple-helix (iC_{H_3}) (Figure S3(a)) to double-helix (iC_{H_2}) (Figure S3(b)) as N_B increases from 4 to 5. The principal mechanism for the formation of the B-helices is that both the cylindrical B-domain and C-domain have their own preferred radii due to the delicate balance between the stretching energy and the interfacial energy, most likely resulting in a noninteger length ratio between the B-cylinder and C-cylinder. Previous works have demonstrated that the B-cylinder of a lower volume fraction should be smaller and longer than the C-cylinder of a higher volume fraction.[83,84] To wrap the longer B-cylinder around the shorter C-cylinder evenly, forming B-helices is an efficient way to accommodate the two cylindrical domains of different lengths into the same structure, so that the length ratio can be continuously tuned by changing the pitch angle of the helices as well as the number of helical strands.[83−85] As N_B increases, the B-helix thickens and its length relative to the C-cylinder decreases, leading to the decrease of helical strands.

https://doi.org/10.1021/acs.macromol.3c00440
Macromolecules XXXX, XXX, XXX−XXX

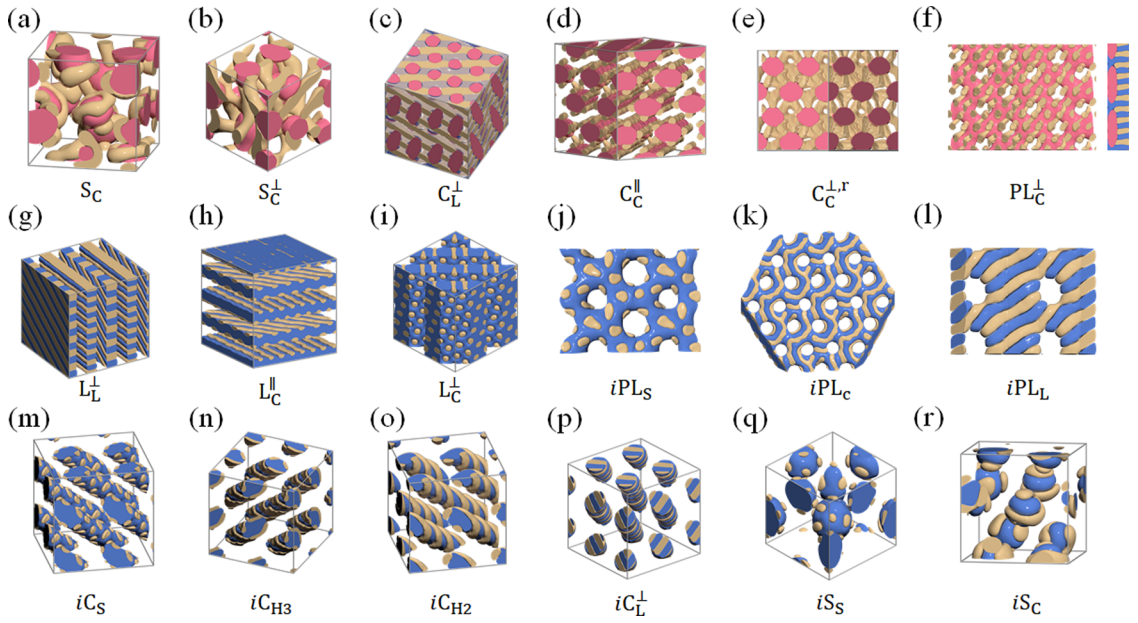

Figure 6. Ordered structures observed in the self-assembly of ABC-type BBCPs. (a) Cylinders-on-spheres (S_C at $n_A = 2$, $N_B = 2$). (b) Cylinders-out-spheres ($S_C^{\perp}$ at $n_A = 2$, $N_B = 3$). (c) Perpendicular lamellae-out-cylinders ($C_L^{\perp}$ at $n_A = 3$, $N_B = 6$). (d) Parallel cylinders-on-cylinders ($C_C^{\parallel}$ at $n_A = 3$, $N_B = 2$). (e) Perpendicular cylinders-out-cylinders ($C_C^{\perp,r}$ at $n_A = 3$, $N_B = 4$). (f) Perpendicular cylinders-out-perforated lamellae ($PL_C^{\perp}$ at $n_A = 4$, $N_B = 3$). (g) Perpendicular lamellae-within-lamellae ($L_L^{\perp}$ at $n_A = 6$, $N_B = 6$). (h) Parallel cylinders-within-lamellae ($L_C^{\parallel}$ at $n_A = 6$, $N_B = 2$). (i) Perpendicular cylinders-within-lamellae ($L_C^{\perp}$ at $n_A = 6$, $N_B = 4$). (j) Spheres-within-inverse perforated lamellae (iPL_S at $n_A = 8$, $N_B = 2$). (k) Cylinders-within-inverse perforated lamellae (iPL_C at $n_A = 8$, $N_B = 3$). (l) Lamellae-within-inverse perforated lamellae (iPL_L at $n_A = 8$, $N_B = 4$). (m) Spheres on inverse cylinders (iC_S at $n_A = 9$, $N_B = 2$). (n) Triple helices-on-inverse cylinders (iC_{H3} at $n_A = 9$, $N_B = 3$). (o) Double helices-on-inverse cylinders (iC_{H2} at $n_A = 9$, $N_B = 5$).(p) Perpendicular lamellae-within-inverse cylinders ($iC_L^{\perp}$ at $n_A = 10$, $N_B = 6$). (q) Spheres-on-inverse spheres (iS_S at $n_A = 10$, $N_B = 2$). (r) Cylinders-on-inverse spheres (iS_C at $n_A = 10$, $N_B = 4$). Only one layer of perforated lamellae is shown for the eye. Red, yellow, and blue represent A, B, and C components, respectively. S, C, L, and H denote spheres, cylinders, lamellae, and helices, respectively.

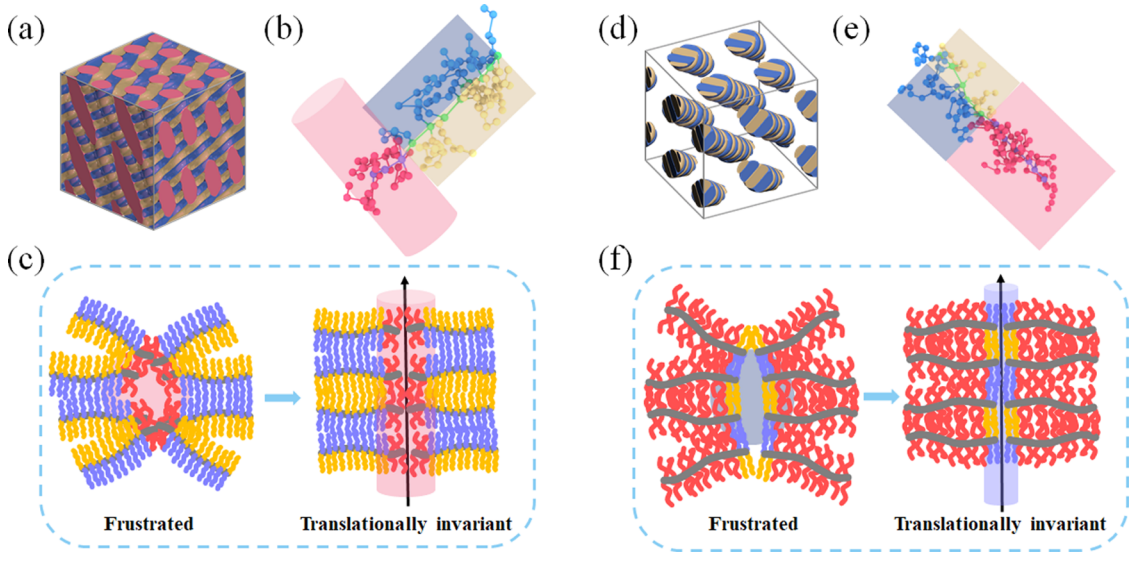

Figure 7. (a) $C_L^{\perp}$ structure ($n_A = 2$, $N_B = 6$), (b) typical chain conformation of the ABC-type bottlebrush copolymer in the $C_L^{\perp}$ structure, (c) schematics illustrating why the A-supercylinder is more favorable for chain packing than the A-supersphere. (d) $iC_L^{\perp}$ structure ($n_A = 10$, $N_B = 6$), (e) typical chain conformation in $iC_L^{\perp}$, (f) analogous schematics to that of (b) for $iC_L^{\perp}$. Red, yellow, and blue represent A, B, and C components, respectively. For reasons of clarity, the backbone beads are divided into (blue) and (green) beads, which are grafted by A beads (red) and B (yellow)/C(blue) beads, respectively.

The formation mechanism of the helices is similar to that in a frustrated ABC linear triblock copolymer melt.[83,86] However, the arrangement of B-helices on the C-cylinder results from the Janus-type bottlebrush architecture of B and C side chains in the ABC-type BBCPs and from the frustrated interactions in the ABC linear triblock architecture.

It is worth noting that some hierarchical structures self-assembled by the ABC-type BBCPs are similar to those formed by ABC star copolymers,[16,87−92] such as $L_L^{\perp}$ and $iC_L^{\perp}$. In these hierarchical structures, symmetric B and C-blocks phase-separate into the substructure of B/C-lamellae embedded in the superstructure of A-lamellae or A-matrix. For the ABC star

https://doi.org/10.1021/acs.macromol.3c00440
Macromolecules XXXX, XXX, XXX−XXX

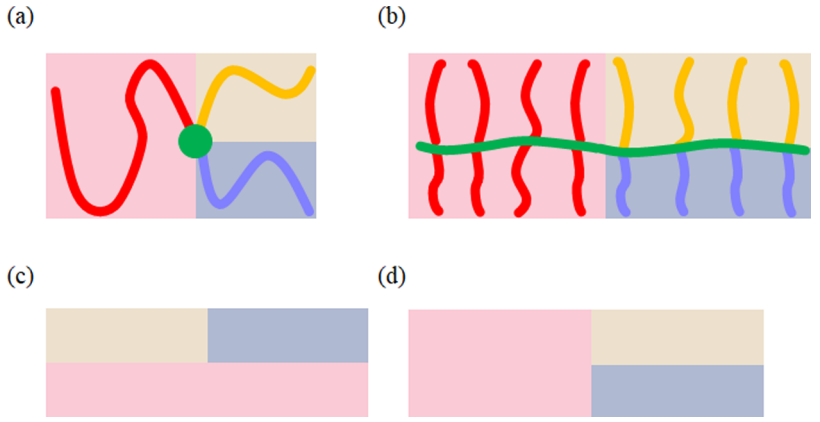

Figure 8. Schematic illustration of molecular packing frustration when ABC star copolymers (a) and ABC-type BBCPs (b) form the lamellae-within-lamellae structure ($L_L^{\perp}$), controlling the domain spacing of the substructure (c) and superstructure (d) by changing the side-chain length and grafted number of side chains, respectively. Red, yellow, and blue represent A, B, and C components and chains. Green represents the junction point of the ABC star copolymer or the backbone of the ABC-type BBCP.

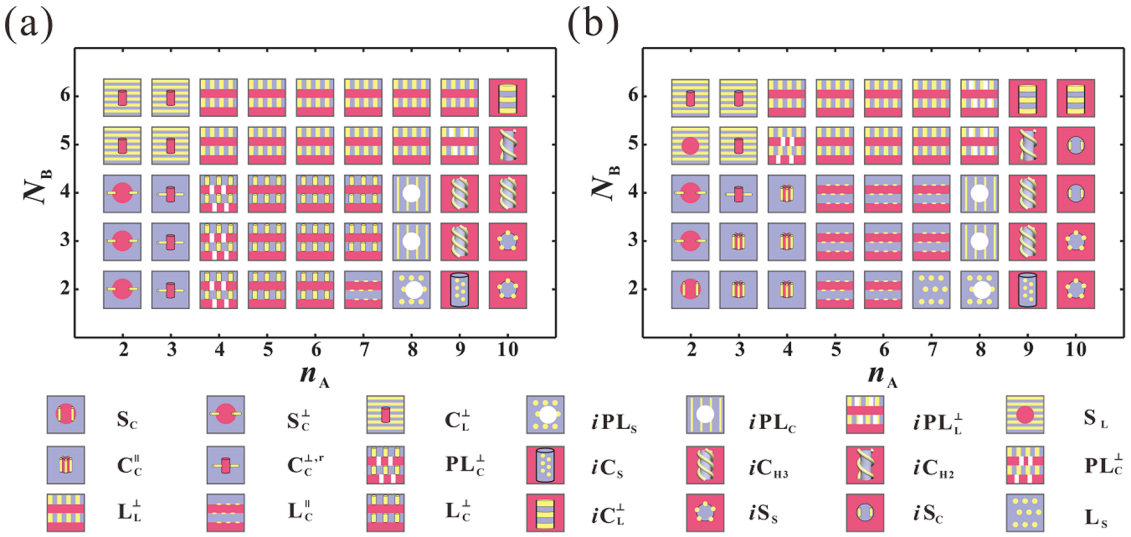

Figure 9. Phase diagrams of ABC-type BBCPs with stiffness parameters k_a = 10 (a) and k_a = 0 (b).

architecture, the junction points have to aggregate at the intersection of A/B, A/C, and B/C interfaces, which constitutes a constraint on the size of the B/C-domain along the direction normal to the interface delimiting the A-domain and the B/C-domain (Figure 8a). In other words, as the volume fractions of B and C-blocks get larger (or the volume fraction of A-block decreases), these perpendicular hierarchical structures tend to transform into polygon-tiling structures where the junction points can readily aggregate at the intersections of three different interfaces. In contrast, for the ABC-type BBCPs, the backbone grafted by B/C-blocks tends to be aligned normal to the interface between the A-domain and B/C-domains and is nearly uniformly distributed on the B/C interface in the perpendicular hierarchical structures (Figure 8b). As a consequence, the size of the B/C-domain along the direction normal to the A-domain depends on the length of the backbone grafted by B/C-blocks, but not the volume fractions of B/C-blocks (Figure 8c,d). These discussions lead to the conclusion that these perpendicular hierarchical structures have larger stable regions with respect to the volume fraction of B/C-block in the ABC-type BBCPs than in the ABC star copolymers. For example, the $L_L^{\perp}$ morphology is observed in the range of the volume fraction of the A block about $0.33 \lesssim f_A \lesssim 0.66$ in the ABC-type BBCPs, while the width of the stable region is about $\Delta f_A \approx 0.2$ for ABC star block copolymers.[90,93] It is necessary to mention that some of the other perpendicular hierarchical structures are difficult to form in ABC star copolymers, such as lamellae-out-cylinders ($C_L^{\perp}$).

Reasonably, those parallel hierarchical structures (e.g., $L_C^{\parallel}$ and $C_C^{\parallel}$) will transfer to their perpendicular counterparts as the backbone becomes more rigid. To demonstrate the transformation, we construct the phase diagram for k_a = 10 (Figure 9a) and compare it with that of k_a = 2. Except for the parameter points of n_a = 7 and N_B = 2, the $L_C^{\parallel}$ structure of all parameter points changes to the $L_C^{\perp}$ structure. The bending angle of the backbone in Figure S4(a) as well as the increased bending energy of the backbone in Figure S5 shows that the transition is driven by the increased bending energy of the backbone. A similar transition is also observed for other structures (Figure S4(b−d)), such as that from $C_C^{\parallel}$ to $C_C^{\perp}$ at n_A = 3 and N_B = 2. Oppositely, we also construct the phase diagram for the flexible backbone with k_a = 0 (Figure 9b). Compared with the phase diagram of k_a = 2, the stable regions

https://doi.org/10.1021/acs.macromol.3c00440
Macromolecules XXXX, XXX, XXX−XXX

of perpendicular hierarchical structures notably contract. Due to the flexibility of the backbone, three new hierarchical structures, lamellae-out-spheres (S_L), perforated lamellae-out-lamellae ($PL_L^{\parallel}$), and oblate spheres-within-lamellae (L_S), are observed at the parameter points of (n_A, N_B) = (2, 5), (4, 5), and (7, 2), respectively (Figure S6).

CONCLUSIONS

We have systemically investigated the self-assembly of ABC-type BBCPs with respect to the number of A side chains n_A, the length of B side chains N_B, as well as the backbone rigidity through dissipative particle dynamics simulations. It is shown that ABC-type BBCPs can spontaneously phase-separate into a variety of hierarchical structures, such as perpendicular lamellae-within-lamellae ($L_L^{\perp}$), perpendicular cylinders-within-lamellae ($L_C^{\perp}$), and perpendicular lamellae-within-inverse cylinders ($iC_L^{\perp}$). Though some of these hierarchical structures are similar to those formed by ABC star copolymers, ABC-type BBCPs exhibit much larger stable parameter regions for them than ABC star copolymers. The main reason is that the junction of the ABC star architecture disfavors the formation of these perpendicular hierarchical structures, while the backbone of BBCPs does not. Moreover, the ABC-type BBCPs can also form some novel hierarchical structures that are hard to form in ABC star copolymers, e.g., lamellae-out-cylinders ($C_L^{\perp}$).

Intuitively, the A-superstructure and B-substructure in the perpendicular hierarchical structure are independently controlled by the volume fraction of the A-block and the volume fraction of the B-block relative to that of the C-block. For example, for symmetric $f_A \sim 0.5$, the A-blocks form the lamellar superstructure, while the B-substructure can be regulated to change from lamellae to cylinders by lowering the f_B. However, this simple scenario does not always hold. We find that the A-superstructure changes along with the transformation of the B-substructure when f_A remains unchanged. Specifically, for f_A = 1/6, the A-superstructure transforms from a sphere to a cylinder accompanied by the change of the B-substructure from a cylinder to a lamella. The transformation of the A-superstructure from a sphere to a cylinder is mainly because the interstitial space outside A-cylinders is translationally invariant along the axial direction of A-cylinders, enabling B/C-lamellae to be perfectly arranged along the axial direction, while the interstitial space outside A-spheres does not have translational invariance along any direction.

Our results demonstrate that the rigidity of the backbone plays an important role in the self-assembly behavior of ABC-type BBCPs. When the backbone is semiflexible, in addition to the perpendicular hierarchical structures, parallel hierarchical structures can also be formed, such as parallel cylinders-within-lamellae ($L_C^{\parallel}$) and cylinders-on-cylinders ($C_C^{\parallel}$). Although the backbone is unfavorably bent, the parallel arrangement of B-substructures on the A/C interface is beneficial to raise the conformational entropy arising from the increased asymmetry between B and C side chains. The formation of parallel hierarchical structures is suppressed by increasing the backbone rigidity. Since our simulations can clearly visualize these complex hierarchical structures, especially the arrangement of the subdomains within the superstructures, this work provides helpful guidance for relevant experiments. One of the most remarkable conclusions is that the transformation of the A-superstructure can be coupled with that of the B-substructure to some extent, which was thought to be completely decoupled in the original experimental work. Furthermore, we found that the coupling degree is affected by the volume fraction of the A side chain.

ASSOCIATED CONTENT

Supporting Information

The Supporting Information is available free of charge at https://pubs.acs.org/doi/10.1021/acs.macromol.3c00440.

Effective Kuhn length b_K of the backbone of the ABC-type BBCPs for k_a = 0, 2, and10 in the disordered state with a_{AB} = a_{AC} = a_{BC} = 25; comparisons of the averaged bending energy per bond of the backbone for the perpendicular hierarchical structures and parallel hierarchical structures; morphological plots for triple helices-on-inverse cylinders (iC_{H3}) (n_A = 9, N_B = 4) and double helices-on-inverse cylinders (iC_{H2}) (n_A = 9, N_B = 5); and comparisons of the averaged bending energy per bond of the backbone for the parallel hierarchical structures (k_a = 2) and perpendicular hierarchical structures (k_a = 10) (PDF)

AUTHOR INFORMATION

Corresponding Authors

Mingjiang Zhong − *Department of Chemistry, Yale University, New Haven, Connecticut 06520, United States; Department of Chemical and Environmental Engineering, Yale University, New Haven, Connecticut 06520, United States;* orcid.org/0000-0001-7533-4708; Email: mingjiang.zhong@yale.edu

Weihua Li − *State Key Laboratory of Molecular Engineering of Polymers, Key Laboratory of Computational Physical Sciences, Department of Macromolecular Science, Fudan University, Shanghai 200433, China;* orcid.org/0000-0002-5133-0267; Email: weihuali@fudan.edu.cn

Authors

Qingliang Song − *State Key Laboratory of Molecular Engineering of Polymers, Key Laboratory of Computational Physical Sciences, Department of Macromolecular Science, Fudan University, Shanghai 200433, China*

Qingshu Dong − *State Key Laboratory of Molecular Engineering of Polymers, Key Laboratory of Computational Physical Sciences, Department of Macromolecular Science, Fudan University, Shanghai 200433, China*

Ruiqi Liang − *Department of Chemical and Environmental Engineering, Yale University, New Haven, Connecticut 06520, United States*

Yazhen Xue − *Department of Chemical and Environmental Engineering, Yale University, New Haven, Connecticut 06520, United States*

Complete contact information is available at: https://pubs.acs.org/10.1021/acs.macromol.3c00440

Notes

The authors declare no competing financial interest.

ACKNOWLEDGMENTS

This work was supported by the National Natural Science Foundation of China (Grant No. 21925301). M.Z. acknowledges support from the National Science Foundation (DMR-2003875)

REFERENCES

(1) Bates, F. S.; Fredrickson, G. H. Block Copolymer Thermodynamics-Theory and Experiment. *Annu. Rev. Phys. Chem.* **1990**, *41*, 525−557.

(2) Hamley, I. W. *The Physics of Block Copolymers*; Oxford University Press: New York, 1998.

(3) Mai, Y. Y.; Eisenberg, A. Self-Assembly of Block Copolymers. *Chem. Soc. Rev.* **2012**, *41*, 5969−5985.

(4) Bates, C. M.; Bates, F. S. 50th Anniversary Perspective: Block Polymers-Pure Potential. *Macromolecules* **2017**, *50*, 3−22.

(5) Leibler, L. Theory of Microphase Separation in Block Co-Polymers. *Macromolecules* **1980**, *13*, 1602−1617.

(6) Matsen, M. W.; Schick, M. Stable and Unstable Phases of a Diblock Copolymer Melt. *Phys. Rev. Lett.* **1994**, *72*, 2660−2663.

(7) Sheiko, S. S.; Sumerlin, B. S.; Matyjaszewski, K. Cylindrical Molecular Brushes: Synthesis, Characterization, and Properties. *Prog. Polym. Sci.* **2008**, *33*, 759−785.

(8) Rzayev, J. Synthesis of Polystyrene-Polylactide Bottlebrush Block Copolymers and Their Melt Self-Assembly into Large Domain Nanostructures. *Macromolecules* **2009**, *42*, 2135−2141.

(9) Gregory, A.; Stenzel, M. H. Complex Polymer Architectures via Raft Polymerization: From Fundamental Process to Extending the Scope Using Click Chemistry and Nature's Building Blocks. *Prog. Polym. Sci.* **2012**, *37*, 38−105.

(10) Polymeropoulos, G.; Zapsas, G.; Ntetsikas, K.; Bilalis, P.; Gnanou, Y.; Hadjichristidis, N. 50th Anniversary Perspective: Polymers with Complex Architectures. *Macromolecules* **2017**, *50*, 1253−1290.

(11) Fei, H.-F.; Yavitt, B. M.; Nuguri, S.; Yu, Y.-G.; Watkins, J. J. Ultrafast Self-Assembly of Bottlebrush Statistical Copolymers: Well-Ordered Nanostructures from One-Pot Polymerizations. *Macromolecules* **2021**, *54*, 10943−10950.

(12) Matsen, M. W. Effect of Architecture on the Phase Behavior of AB-Type Block Copolymer Melts. *Macromolecules* **2012**, *45*, 2161−2165.

(13) Bates, F. S.; Hillmyer, M. A.; Lodge, T. P.; Bates, C. M.; Delaney, K. T.; Fredrickson, G. H. Multiblock Polymers: Panacea or Pandora's Box? *Science* **2012**, *336*, 434−440.

(14) Fei, H. F.; Yayitt, B. M.; Hu, X. Y.; Kopanati, G.; Ribbe, A.; Watkins, J. J. Influence of Molecular Architecture and Chain Flexibility on the Phase Map of Polystyrene-Block-Poly-(Dimethylsiloxane) Brush Block Copolymers. *Macromolecules* **2019**, *52*, 6449−6457.

(15) Hayashida, K.; Takano, A.; Arai, S.; Shinohara, Y.; Amemiya, Y.; Matsushita, Y. Systematic Transitions of Tiling Patterns Formed by ABC Star-Shaped Terpolymers. *Macromolecules* **2006**, *39*, 9402−9408.

(16) Hayashida, K.; Saito, N.; Arai, S.; Takano, A.; Tanaka, N.; Matsushita, Y. Hierarchical Morphologies Formed by ABC Star-Shaped Terpolymers. *Macromolecules* **2007**, *40*, 3695−3699.

(17) Hayashida, K.; Dotera, T.; Takano, A.; Matsushita, Y. Polymeric Quasicrystal: Mesoscopic Quasicrystalline Tiling in ABC Star Polymers. *Phys. Rev. Lett.* **2007**, *98*, No. 195502.

(18) Miyamori, Y.; Suzuki, J.; Takano, A.; Matsushita, Y. Periodic and Aperiodic Tiling Patterns from a Tetrablock Terpolymer System of the A_1BA_2C Type. *ACS Macro Lett.* **2020**, *9*, 32−37.

(19) Yoon, H.; Ahn, S.; Dong, Q. S.; Choi, C.; Kim, E.; Li, W. H.; Kim, J. K. Multidomain Helical Nanostructure by A_1BA_2C Tetrablock Terpolymer Self-Assembly. *ACS Macro Lett.* **2021**, *10*, 1119−1124.

(20) Seo, Y.; Woo, D.; Li, L. Y.; Li, W. H.; Kim, J. K. Phase Behavior of PS-(PS-*b*-P2VP)$_3$ Miktoarm Star Copolymer. *Macromolecules* **2021**, *54*, 7822−7829.

(21) Seo, Y.; Park, S. Y.; Lee, J.; Kim, J. K.; Duan, C.; Li, W. H. Inverted Cylindrical Microdomains by Blending Star-Shaped and Linear Block Copolymers. *Macromolecules* **2021**, *54*, 629−636.

(22) Ahn, S.; Yoon, H.; Duan, C.; Li, W. H.; Kim, J. K. Core-Satellite Micelles by a Linear $A_1B_1A_2B_2$ Tetrablock Copolymer. *Macromolecules* **2022**, *55*, 1544−1551.

(23) Suzuki, M.; Orido, T.; Takano, A.; Matsushita, Y. The Largest Quasicrystalline Tiling with Dodecagonal Symmetry from a Single Pentablock Quarterpolymer of the AB_1CB_2D Type. *ACS Nano* **2022**, *16*, 6111−6117.

(24) Zhang, G. J.; Qiu, F.; Zhang, H. D.; Yang, Y. L.; Shi, A.-C. SCFT Study of Tiling Patterns in ABC Star Terpolymers. *Macromolecules* **2010**, *43*, 2981−2989.

(25) Qin, J.; Bates, F. S.; Morse, D. C. Phase Behavior of Nonfrustrated ABC Triblock Copolymers: Weak and Intermediate Segregation. *Macromolecules* **2010**, *43*, 5128−5136.

(26) Wang, L. Q.; Lin, J. P.; Zhang, L. S. Hierarchically Ordered Microstructures Self-Assembled from A(BC)*n* Multiblock Copolymers. *Macromolecules* **2010**, *43*, 1602−1609.

(27) Xie, N.; Li, W. H.; Qiu, F.; Shi, A.-C. σ Phase Formed in Conformationally Asymmetric AB-Type Block Copolymers. *ACS Macro Lett.* **2014**, *3*, 906−910.

(28) Li, W. H.; Duan, C.; Shi, A.-C. Nonclassical Spherical Packing Phases Self-Assembled from AB-Type Block Copolymers. *ACS Macro Lett.* **2017**, *6*, 1257−1262.

(29) Chremos, A.; Theodorakis, P. E. Morphologies of Bottle-Brush Block Copolymers. *ACS Macro Lett.* **2014**, *3*, 1096−1100.

(30) Duan, C.; Zhao, M. T.; Qiang, Y. C.; Chen, L.; Li, W. H.; Qu, F.; Shi, A.-C. Stability of Two-Dimensional Dodecagonal Quasicrystalline Phase of Block Copolymers. *Macromolecules* **2018**, *51*, 7713−7721.

(31) Lequieu, J.; Quah, T.; Delaney, K. T.; Fredrickson, G. H. Complete Photonic Band Gaps with Nonfrustrated ABC Bottlebrush Block Polymers. *ACS Macro Lett.* **2020**, *9*, 1074−1080.

(32) Xu, Z. W.; Li, W. H. Control the Self-Assembly of Block Copolymers by Tailoring the Packing Frustration. *Chin. J. Chem.* **2022**, *40*, 1083−1090.

(33) Xie, Q.; Qiang, Y. C.; Li, W. H. Single Gyroid Self-Assembled by Linear BABAB Pentablock Copolymer. *ACS Macro Lett.* **2022**, *11*, 205−209.

(34) Xie, N.; Liu, M. J.; Deng, H. L.; Li, W. H.; Qiu, F.; Shi, A.-C. Macromolecular Metallurgy of Binary Mesocrystals via Designed Multiblock Terpolymers. *J. Am. Chem. Soc.* **2014**, *136*, 2974−2977.

(35) Gao, Y.; Deng, H. L.; Li, W. H.; Qiu, F.; Shi, A.-C. Formation of Nonclassical Ordered Phases of AB-Type Multiarm Block Copolymers. *Phys. Rev. Lett.* **2016**, *116*, No. 068304.

(36) Qiang, Y. C.; Li, W. H.; Shi, A.-C. Stabilizing Phases of Block Copolymers with Gigantic Spheres via Designed Chain Architectures. *ACS Macro Lett.* **2020**, *9*, 668−673.

(37) Lequieu, J.; Koeper, T.; Delaney, K. T.; Fredrickson, G. H. Extreme Deflection of Phase Boundaries and Chain Bridging in A(BA′)*n* Miktoarm Star Polymers. *Macromolecules* **2020**, *53*, 513−522.

(38) Li, C. C.; Dong, Q. S.; Li, W. H. Largely Tunable Asymmetry of Phase Diagrams of A(AB)*n* Miktoarm Star Copolymer. *Macromolecules* **2020**, *53*, 10907−10917.

(39) Song, Q. L.; Dong, Q. S.; Dong, X.-H.; Zhu, Y.-L.; Li, W. H. Self-Assembly Behaviors of Giant Amphiphiles Containing Cubic Cage-Like "Monomers. *Macromolecules* **2021**, *54*, 8601−8611.

(40) Xie, Q.; Qiang, Y. C.; Chen, L.; Xia, Y. M.; Li, W. H. Synergistic Effect of Stretched Bridging Block and Released Packing Frustration Leads to Exotic Nanostructures. *ACS Macro Lett.* **2020**, *9*, 980−984.

(41) Ahn, S.; Kim, J. K.; Zhao, B.; Duan, C.; Li, W. H. Morphology Transitions of Linear $A_1B_1A_2B_2$ Tetrablock Copolymers at Symmetric Overall Volume Fraction. *Macromolecules* **2018**, *51*, 4415−4421.

(42) Bolton, J.; Rzayev, J. Synthesis and Melt Self-Assembly of PS-PMMA-PLA Triblock Bottlebrush Copolymers. *Macromolecules* **2014**, *47*, 2864−2874.

(43) Kawamoto, K.; Zhong, M.; Gadelrab, K. R.; Cheng, L.-C.; Ross, C. A.; Alexander-Katz, A.; Johnson, J. A. Graft-through Synthesis and Assembly of Janus Bottlebrush Polymers from A-Branch-B Diblock Macromonomers. *J. Am. Chem. Soc.* **2016**, *138*, 11501−11504.

(44) Park, S. J.; Cheong, G. K.; Bates, F. S.; Dorfman, K. D. Stability of the Double Gyroid Phase in Bottlebrush Diblock Copolymer Melts. *Macromolecules* **2021**, *54*, 9063−9070.

https://doi.org/10.1021/acs.macromol.3c00440
Macromolecules XXXX, XXX, XXX−XXX

(45) Cui, S. Q.; Zhang, B.; Shen, L. Y.; Bates, F. S.; Lodge, T. P. Core-Shell Gyroid in ABC Bottlebrush Block Terpolymers. *J. Am. Chem. Soc.* **2022**, *144*, 21719−21727.
(46) Liberman, L.; Coughlin, M. L.; Weigand, S.; Bates, F. S.; Lodge, T. P. Phase Behavior of Linear-Bottlebrush Block Polymers. *Macromolecules* **2022**, *55*, 2821−2831.
(47) Liang, R. Q.; Xue, Y. Z.; Fu, X. W.; Le, A. N.; Song, Q. L.; Qiang, Y. C.; Xie, Q.; Dong, R. Q.; Sun, Z. H.; Osuji, C. O.; Johnson, J. A.; Li, W. H.; Zhong, M. J. Hierarchically Engineered Nanostructures from Compositionally Anisotropic Molecular Building Blocks. *Nat. Mater.* **2022**, *21*, 1434−1440.
(48) Liang, R. Q.; Song, Q. L.; Li, R. P.; Le, A. N.; Fu, X. W.; Xue, Y. Z.; Ji, X. Y.; Li, W. H.; Zhong, M. J. Rapid Access to Diverse Multicomponent Hierarchical Nanostructures from Mixed-Graft Block Copolymers. *Angew. Chem., Int. Ed.* **2022**, *61*, No. e202210067.
(49) Vigil, D. L.; Quah, T.; Sun, D.; Delaney, K. T.; Fredrickson, G. H. Self-Consistent Field Theory Predicts Universal Phase Behavior for Linear, Comb, and Bottlebrush Diblock Copolymers. *Macromolecules* **2022**, *55*, 4237−4244.
(50) Chen, D.; Quah, T.; Delaney, K. T.; Fredrickson, G. H. Investigation of the Self-Assembly Behavior of Statistical Bottlebrush Copolymers via Self-Consistent Field Theory Simulations. *Macromolecules* **2022**, *55*, 9324−9333.
(51) Sun, Z. H.; Liu, R. Z.; Su, T. Y.; Huang, H. J.; Kawamoto, K.; Liang, R. Q.; Liu, B.; Zhong, M. J.; Alexander-Katz, A.; Ross, C. A.; Johnson, J. A. Emergence of Layered Nanoscale Mesh Networks through Intrinsic Molecular Confinement Self-Assembly. *Nat. Nanotechnol.* **2023**, *18*, 273−280.
(52) Xia, Y.; Olsen, B. D.; Kornfield, J. A.; Grubbs, R. H. Efficient Synthesis of Narrowly Dispersed Brush Copolymers and Study of Their Assemblies: The Importance of Side-Chain Arrangement. *J. Am. Chem. Soc.* **2009**, *131*, 18525−18532.
(53) Verduzco, R.; Li, X.; Peseka, S. L.; Steinc, G. E. Structure, Function, Self-Assembly, and Applications of Bottlebrush Copolymers. *Chem. Soc. Rev.* **2015**, *44*, 2405−2420.
(54) Xie, G. J.; Martinez, M. R.; Olszewski, M.; Sheiko, S. S.; Matyjaszewski, K. Molecular Bottlebrushes as Novel Materials. *Biomacromolecules* **2019**, *20*, 27−54.
(55) Kim, E. J.; Shin, J. J.; Do, T.; Lee, G. S.; Park, J.; Thapar, V.; Choi, J.; Bang, J.; Yi, G. R.; Hur, S. M.; Kim, J. G.; Kim, B. J. Molecular Weight Dependent Morphological Transitions of Bottlebrush Block Copolymer Particles: Experiments and Simulations. *ACS Nano* **2021**, *15*, 5513−5522.
(56) Zhao, B. Shape-Changing Bottlebrush Polymers. *J. Phys. Chem. B* **2021**, *125*, 6373−6389.
(57) Salinas-Soto, C. A.; Leon-Islas, J. G.; Herrera-Alonso, M.; Ramírez-Hernández, A. Hydrophobic Solute Encapsulation by Amphiphilic Mikto-Grafted Bottlebrushes: A Dissipative Particle Dynamics Study. *ACS Appl. Polym. Mater.* **2022**, *4*, 7340−7351.
(58) Park, J.; Thapar, V.; Choe, Y.; Salas, L. A. P.; Ramírez-Hernández, A.; de Pablo, J. J.; Hur, S.-M. Coarse-Grained Simulation of Bottlebrush: From Single-Chain Properties to Self-Assembly. *ACS Macro Lett.* **2022**, *11*, 1167−1173.
(59) Dalsin, S. J.; Rions-Maehren, T. G.; Beam, M. D.; Bates, F. S.; Hillmyer, M. A.; Matsen, M. W. Bottlebrush Block Polymers: Quantitative Theory and Experiments. *ACS Nano* **2015**, *9*, 12233−12245.
(60) Gai, Y.; Song, D. P.; Yavitt, B. M.; Watkins, J. J. Polystyrene-Block-Poly(Ethylene Oxide) Bottlebrush Block Copolymer Morphology Transitions: Influence of Side Chain Length and Volume Fraction. *Macromolecules* **2017**, *50*, 1503−1511.
(61) Fei, H. F.; Yavitt, B. M.; Kopanati, G.; Watkins, J. J. Effect of Side Chain and Backbone Length on Lamellar Spacing in Polystyrene-Block-Poly(Dimethyl Siloxane) Brush Block Copolymers. *J. Polym. Sci., Part B: Polym. Phys.* **2019**, *57*, 691−699.
(62) Sveinbjörnsson, B. R.; Weitekamp, R. A.; Miyake, G. M.; Xia, Y.; Atwater, H. A.; Grubbs, R. H. Rapid Self-Assembly of Brush Block Copolymers to Photonic Crystals. *Proc. Natl. Acad. Sci. U.S.A.* **2012**, *109*, 14332−14336.
(63) Liberman-Martin, A. L.; Chu, C. K.; Grubbs, R. H. Application of Bottlebrush Block Copolymers as Photonic Crystals. *Macromol. Rapid Commun.* **2017**, *38*, No. 1700058.
(64) Wang, Q.; Gu, K. H.; Zhang, Z. Y.; Hou, P. P.; Shen, Z. H.; Fan, X. H. Morphologies and Photonic Properties of an Asymmetric Brush Block Copolymer with Polystyrene and Polydimethylsiloxane Side Chains. *Polymer* **2018**, *156*, 169−178.
(65) Vatankhah-Varnosfaderani, M.; Keith, A. N.; Cong, Y.; Liang, H.; Rosenthal, M.; Sztucki, M.; Clair, C.; Magonov, S.; Ivanov, D. A.; Dobrynin, A. V.; Sheiko, S. S. Chameleon-Like Elastomers with Molecularly Encoded Strain-Adaptive Stiffening and Coloration. *Science* **2018**, *359*, 1509−1513.
(66) Song, D.-P.; Zhao, T. H.; Guidetti, G.; Vignolini, S.; Parker, R. M. Hierarchical Photonic Pigments via the Confined Self-Assembly of Bottlebrush Block Copolymers. *ACS Nano* **2019**, *13*, 1764−1771.
(67) Song, D.-P.; Li, C.; Colella, N. S.; Lu, X. M.; Lee, J. H.; Watkins, J. J. Thermally Tunable Metallodielectric Photonic Crystals from the Self-Assembly of Brush Block Copolymers and Gold Nanoparticles. *Adv. Opt. Mater.* **2015**, *3*, 1169−1175.
(68) Song, D.-P.; Li, C.; Li, W. H.; Watkins, J. J. Block Copolymer Nanocomposites with High Refractive Index Contrast for One-Step Photonics. *ACS Nano* **2016**, *10*, 1216−1223.
(69) Guo, Z. H.; Le, A. N.; Feng, X. D.; Choo, Y.; Liu, B. Q.; Wang, D. Y.; Wan, Z. Y.; Gu, Y. W.; Zhao, J.; Li, V.; Osuji, C. O.; Johnson, J. A.; Zhong, M. J. Janus Graft Block Copolymers: Design of a Polymer Architecture for Independently Tuned Nanostructures and Polymer Properties. *Angew. Chem., Int. Ed.* **2018**, *57*, 8493−8497.
(70) Gadelrab, K. R.; Alexander-Katz, A. Effect of Molecular Architecture on the Self-Assembly of Bottlebrush Copolymers. *J. Phys. Chem. B* **2020**, *124*, 11519−11529.
(71) Liu, R. Z.; Sun, Z. H.; Huang, H. J.; Johnson, J. A.; Alexander-Katz, A.; Ross, C. A. Experimental and Computational Evaluation of Self-Assembled Morphologies in Diblock Janus Bottlebrush Copolymers. *Nano Lett.* **2023**, *23*, 177−182.
(72) Hoogerbrugge, P. J.; Koelman, J. Simulating Microscopic Hydrodynamic Phenomena with Dissipative Particle Dynamics. *Europhys. Lett.* **1992**, *19*, 155−160.
(73) Español, P.; Warren, P. Statistical-Mechanics of Dissipative Particle Dynamics. *Europhys. Lett.* **1995**, *30*, 191−196.
(74) Groot, R. D.; Warren, P. B. Dissipative Particle Dynamics: Bridging the Gap between Atomistic and Mesoscopic Simulation. *J. Chem. Phys.* **1997**, *107*, 4423−4435.
(75) Groot, R. D.; Madden, T. J. Dynamic Simulation of Diblock Copolymer Microphase Separation. *J. Chem. Phys.* **1998**, *108*, 8713−8724.
(76) Saito, N.; Takahashi, K.; Yunoki, Y. Statistical Mechanical Theory of Stiff Chains. *J. Phys. Soc. Jpn.* **1967**, *22*, 219−226.
(77) Horsch, M. A.; Zhang, Z. L.; Iacovella, C. R.; Glotzer, S. C. Hydrodynamics and Microphase Ordering in Block Copolymers: Are Hydrodynamics Required for Ordered Phases with Periodicity in More Than One Dimension? *J. Chem. Phys.* **2004**, *121*, 11455−11462.
(78) Feng, Y.; Li, B. H.; Wang, Q. Finding the Bulk Periodicity of Lamellar and Cylindrical Structures Using the Pressure Tensor. *Soft Matter* **2022**, *18*, 4923−4929.
(79) Feng, Y.; Wu, J. P.; Li, B. H.; Wang, Q. Periodicity and Global Order Parameter of Hexagonally Packed Cylinders in a Periodic Box. *Soft Matter* **2022**, *18*, 2750−2756.
(80) Zhu, Y.-L.; Liu, H.; Li, Z. W.; Qian, H. J.; Milano, G.; Lu, Z. Y. GALAMOST: GPU-Accelerated Large-Scale Molecular Simulation Toolkit. *J. Comput. Chem.* **2013**, *34*, 2197−2211.
(81) Liang, H. Y.; Cao, Z.; Wang, Z. L.; Sheiko, S. S.; Dobrynin, A. V. Combs and Bottlebrushes in a Melt. *Macromolecules* **2017**, *50*, 3430−3437.
(82) Daoulas, K. C.; Muller, M.; Stoykovich, M. P.; Park, S. M.; Papakonstantopoulos, Y. J.; de Pablo, J. J.; Nealey, P. F.; Solak, H. H. Fabrication of Complex Three-Dimensional Nanostructures from Self-Assembling Block Copolymer Materials on Two-Dimensional Chemically Patterned Templates with Mismatched Symmetry. *Phys. Rev. Lett.* **2006**, *96*, No. 036104.

https://doi.org/10.1021/acs.macromol.3c00440
Macromolecules XXXX, XXX, XXX−XXX

(83) Li, W. H.; Qiu, F.; Shi, A.-C. Emergence and Stability of Helical Superstructures in ABC Triblock Copolymers. *Macromolecules* **2012**, *45*, 503−509.
(84) Zhang, Q.; Qiang, Y. C.; Duan, C.; Li, W. H. Single Helix Self-Assembled by Frustrated ABC_2 Branched Terpolymers. *Macromolecules* **2019**, *52*, 2748−2758.
(85) Yu, B.; Sun, P. C.; Chen, T. H.; Jin, Q. H.; Ding, D. T.; Li, B. H.; Shi, A. C. Confinement-Induced Novel Morphologies of Block Copolymers. *Phys. Rev. Lett.* **2006**, *96*, No. 138306.
(86) Jinnai, H.; Kaneko, T.; Matsunaga, K.; Abetz, C.; Abetz, V. A Double Helical Structure Formed from an Amorphous, Achiral ABC Triblock Terpolymer. *Soft Matter* **2009**, *5*, 2042−2046.
(87) Gemma, T.; Hatano, A.; Dotera, T. Monte Carlo Simulations of the Morphology of ABC Star Polymers Using the Diagonal Bond Method. *Macromolecules* **2002**, *35*, 3225−3237.
(88) Tang, P.; Qiu, F.; Zhang, H. D.; Yang, Y. L. Morphology and Phase Diagram of Complex Block Copolymers: ABC Star Triblock Copolymers. *J. Phys. Chem. B* **2004**, *108*, 8434−8438.
(89) Takano, A.; Kawashima, W.; Wada, S.; Hayashida, K.; Sato, S.; Kawahara, S.; Isono, Y.; Makihara, M.; Tanaka, N.; Kawaguchi, D.; Matsushita, Y. Composition Dependence of Nanophase-Separated Structures Formed by Star-Shaped Terpolymers of the $A_{1.0}B_{1.0}C_x$ Type. *J. Polym. Sci., Part B: Polym. Phys.* **2007**, *45*, 2277−2283.
(90) Li, W. H.; Xu, Y. C.; Zhang, G. J.; Qiu, F.; Yang, Y. L.; Shi, A.-C. Real-Space Self-Consistent Mean-Field Theory Study of ABC Star Triblock Copolymers. *J. Chem. Phys.* **2010**, *133*, No. 064904.
(91) Matsushita, Y.; Hayashida, K.; Dotera, T.; Takano, A. Kaleidoscopic Morphologies from ABC Star-Shaped Terpolymers. *J. Phys.: Condens. Matter* **2011**, *23*, No. 284111.
(92) Jiang, K.; Zhang, J.; Liang, Q. Self-Assembly of Asymmetrically Interacting ABC Star Triblock Copolymer Melts. *J. Phys. Chem. B* **2015**, *119*, 14551−14562.
(93) Huang, C.-I.; Fang, H.-K.; Lin, C.-H. Morphological Transition Behavior of ABC Star Copolymers by Varying the Interaction Parameters. *Phys. Rev. E* **2008**, *77*, No. 031804.

https://doi.org/10.1021/acs.macromol.3c00440
Macromolecules XXXX, XXX, XXX−XXX